Supporting Information

Epitaxial Welding of Carbon Nanotube Networks for Aqueous Battery Current Collectors

Yonggang Yao,[1,a] Feng Jiang,[1,a] Chongyin Yang,[2] Kun Kelvin Fu,[1] John Hayden,[1] Chuan-Fu Lin,[1] Hua Xie,[1] Miaolun Jiao,[1] Chunpeng Yang,[1] Yilin Wang,[1] Shuaiming He,[1] Fujun Xu,[1] Emily Hitz,[1] Tingting Gao,[1] Jiaqi Dai,[1] Wei Luo,[1] Gary Rubloff,[1] Chunsheng Wang,[2] Liangbing Hu[1,*]

1. Department of Materials Science and Engineering, University of Maryland, College Park, Maryland, 20742
2. Department of Chemical and Biomolecular Engineering, University of Maryland, College Park, Maryland, 20742

[*] Email: binghu@umd.edu

[a] These authors contributed equally to this work.

Microstructure of CNT and CNT-PAN

Fig. S1 displays the SEM and TEM images of pristine CNT film with a porous structure and tube diameters around 30-40 nm. Also, from these TEM images, the CNTs are individually separated with each other without forming chemical bonds or effective connection points.

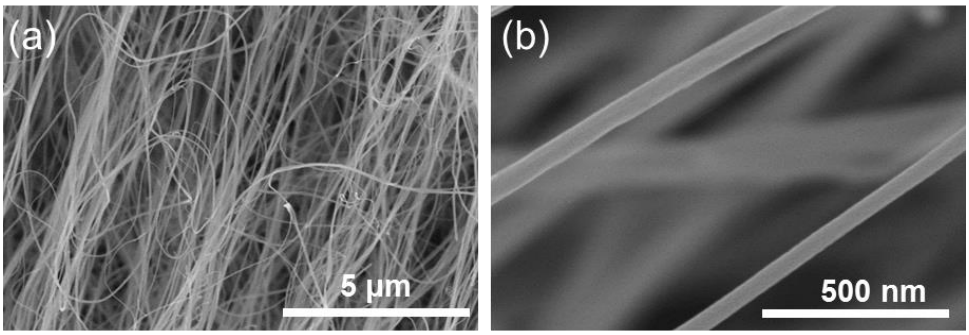

Figure S1. (a)-(b) SEM of pristine dry-processed CNT film.

In Fig. S2, TEM images show the fiber diameter distributions in the pristine CNT film.

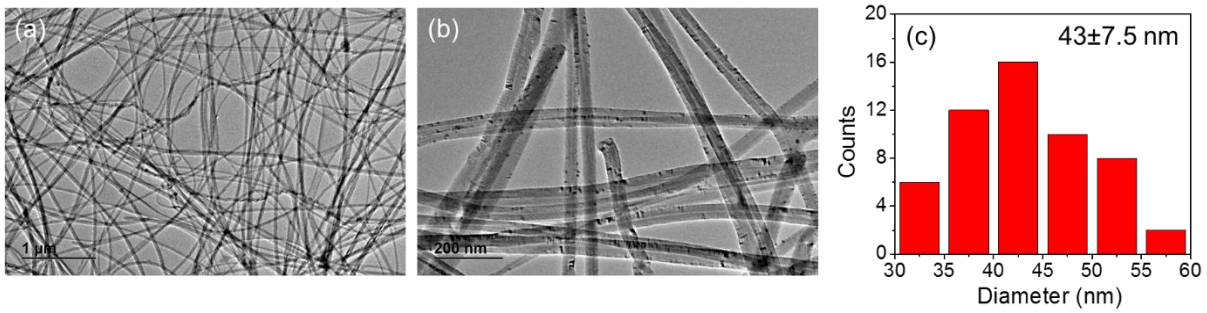

Figure S2. (a)-(b) TEM images of pristine CNT, and (c) statistical analysis of CNT diameter distribution in pristine CNT.

Fig. S3 shows the SEM images of CNT after dipping in a 2% polyacrylonitrile (PAN) solution. The surface of the CNT-PAN film shows a relatively compact configuration, revealing the important characteristic that the CNTs are glued together by the infiltrated PAN polymer.

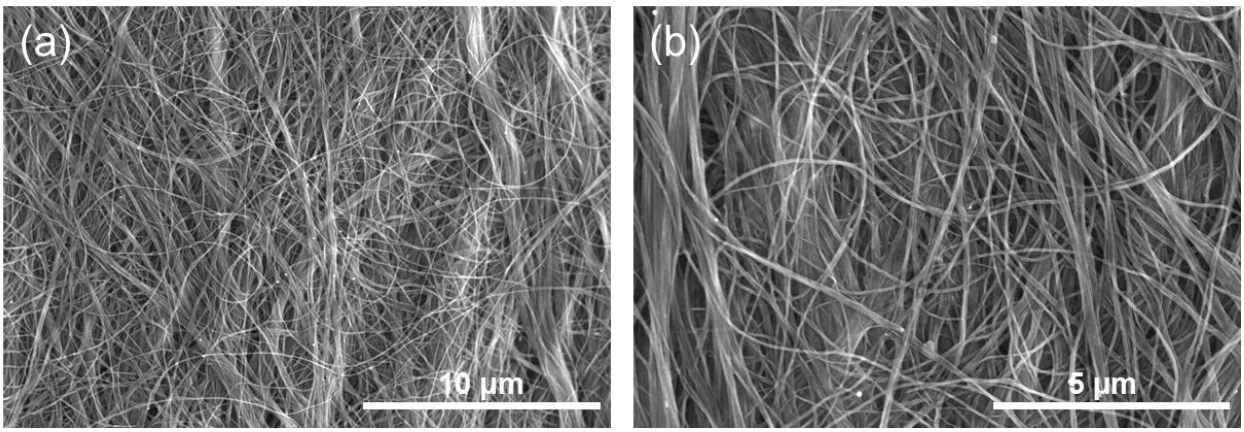

Figure S3. (a)-(b) SEM images of PAN coated CNT (CNT-PAN).

Fig. S4 shows the morphology evolution from CNT to CNT-PAN. The CNT-PAN film shows a much denser structure as the PAN coating layer holds CNTs together after drying with pressing. Also, it is clear that the previous 20-30 μm CNT film becomes ~ 10 μm film in CNT-PAN film. The dense structure improves the contact between CNTs and also renders improved performances such as conductivity and mechanical properties.

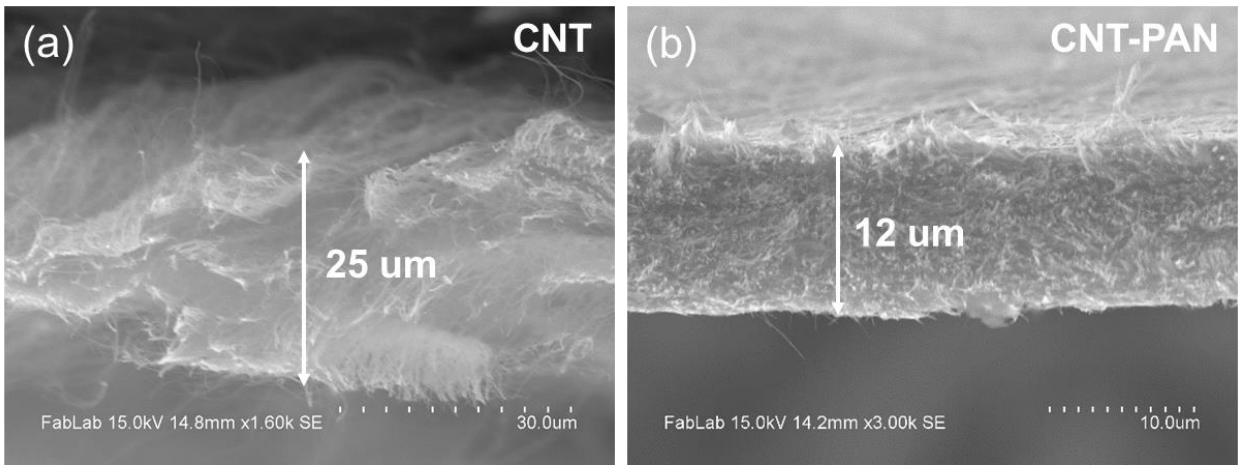

Figure S4. (a)-(b) SEM images of pristine CNT film and CNT-PAN film at the cross-section.

High temperature annealing process

The CNT-PAN samples were Joule heated to high temperature by slowly applying a current across the sample from 0 A to 3.15 A at a step size of 0.001A/s-0.005A/s by programmable LabVIEW module. Below Fig. S5 shows typical heating curves of (a) driven current as a function of time and (b) measured voltage as a function of driven current. It is clear that the V-I curve deviates from the linear relation of a pure resistor; instead, it shows a continuously sublinear evolution, most notably after current reaches above 1.5 A. The deviation from a linear relationship is a strong indication of decreasing resistance during the high temperature annealing process. It is worth noting that during the cooling process after high temperature annealing, the V-I curve is a straight line, showing a relatively constant resistance after annealing.

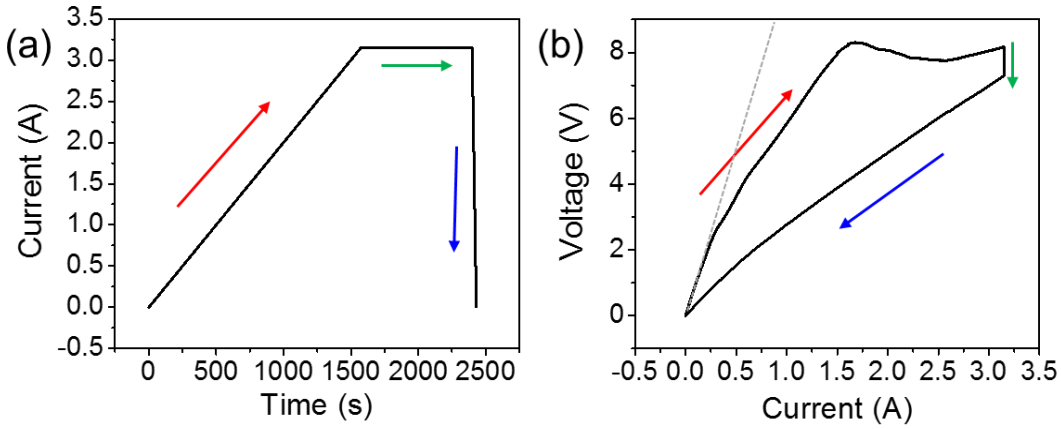

Figure S5. The high temperature annealing process. (a) Current as a function of time and (b) Measured voltage as a function of driven current.

XRD and Raman analysis

Fig. S6a shows the XRD profiles for pristine CNT, CNT-PAN, and W-CNT films. The (002) peak for graphitic carbon is obvious as compared to the control sample (873 K carbonized carbon nanofibers (CNF)). For all the three CNT samples, the peak widths are narrow, indicating high crystallinity in these samples. Note that although CNT-PAN has a sharp peak, the peak intensity is substantially lower than CNT and W-CNT. This is because the amorphous PAN coating on top of CNTs can weaken the crystalline signal beneath.

Fig. S6b shows the Raman profiles for pristine CNT, CNT-PAN, and W-CNT films. The evolution of characteristic D and G peak is evident. After high temperature annealing, the D peak of W-CNT is much smaller with a D:G ratio of 0.06 as compared to the 0.3 D:G ratio for the pristine CNT. The substantial decrease in D:G ratio demonstrates the increase of crystallinity after high temperature annealing. All these CNT samples have a much smaller D:G ratio as compared with the control sample (1.14, low T carbonized CNF) and therefore have higher crystallinity. Note that for CNT-PAN sample, the signal has a large scattered background due to the PAN polymer coating that obscures the real D and G peaks.

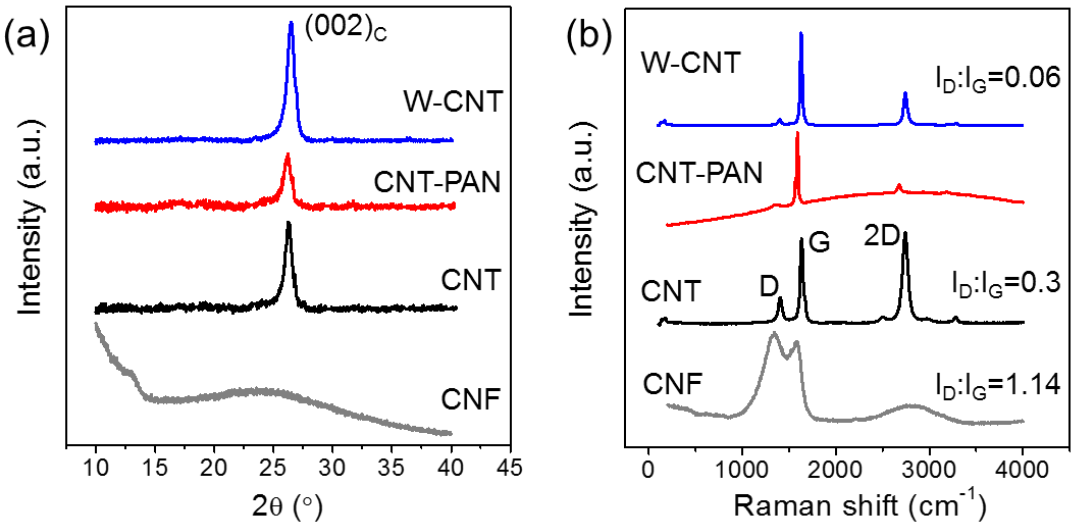

Figure S6. (a) XRD profiles for pristine CNT, CNT-PAN, W-CNT, and a control sample: low temperature (873K) carbonized CNF. The high crystallinity of W-CNT can be indicated by the sharp crystalline (002) peak in the XRD profile. (b) Raman spectra for pristine CNT, CNT-PAN, W-CNT, and CNF. The high crystallinity of W-CNT can be indicated by the low intensity of D peak as well as the low D:G ratio.

Epitaxial growth of CNT

Below shows TEM images of a pristine CNT (Fig. S7a) and a W-CNT partially coated with graphitic layers (Fig. S7b). From the partially coated CNT, the graphitic coating is clear with coating thickness around 10-15 nm. The boundaries between the embedded CNT and the formed graphitic layers are also clearer at the broken coating edge. Fig. S7c and S7d display more clear epitaxial growth in W-CNTs. At higher magnification, the growth pattern of the graphitic layer can be very similar with the embedded CNTs (i.e. “epitaxial growth). Fig. S7d shows a typical high resolution TEM image to demonstrate the epitaxial layer that are almost perfectly aligned with embedded CNTs, confirming an “epitaxial growth” process.

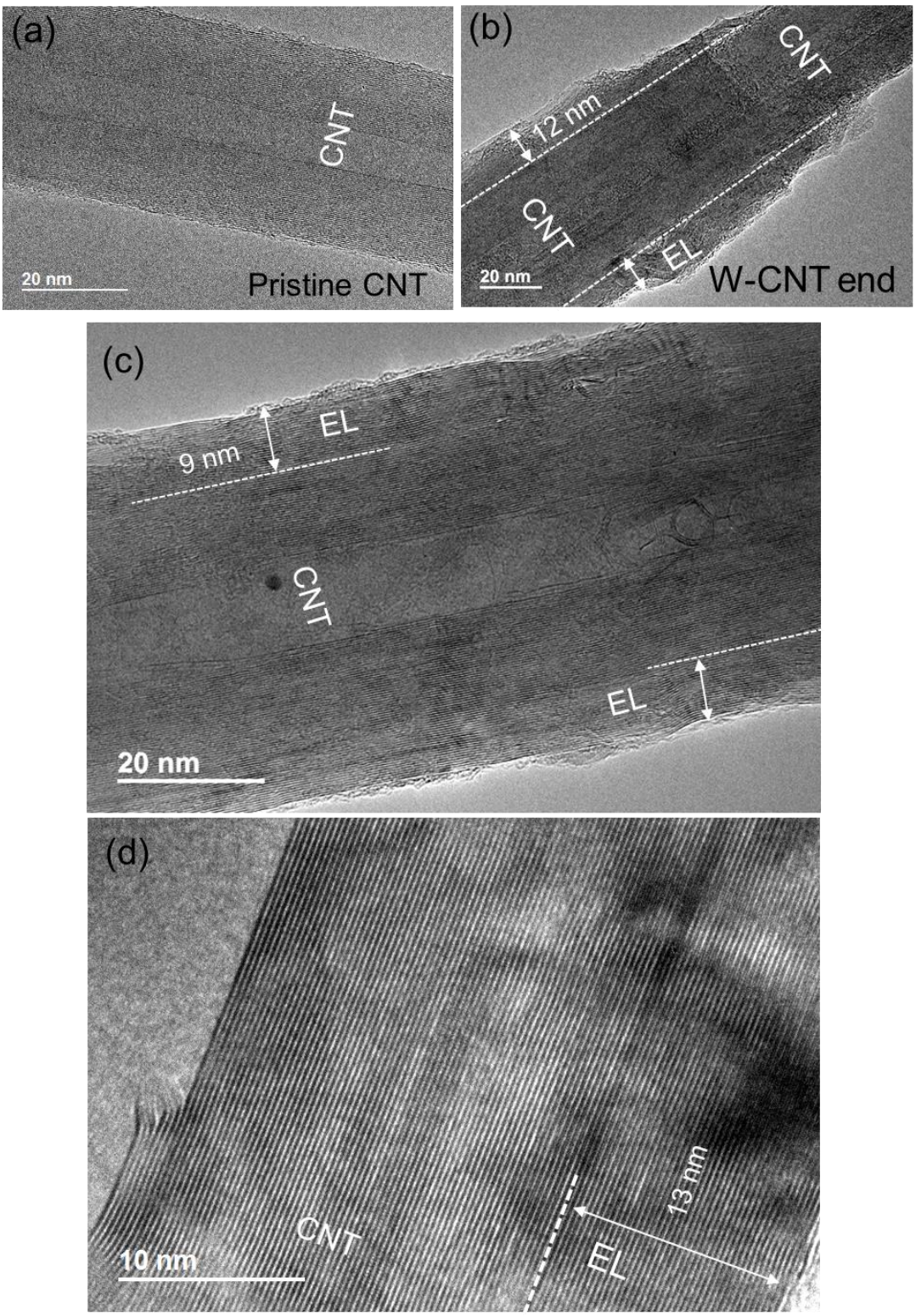

Figure S7. TEM images of (a) pristine CNT and (b) W-CNT with a broken coating which clearly shows the coating thickness to be around 10 nm. (c)-(d) Epitaxial growth of CNTs after polymer glue coating and high temperature annealing. EL stands for epitaxial layers.

Fig. S8 displays the low magnification of W-CNT film and the distribution of fiber diameters after PAN coating and high temperature annealing.

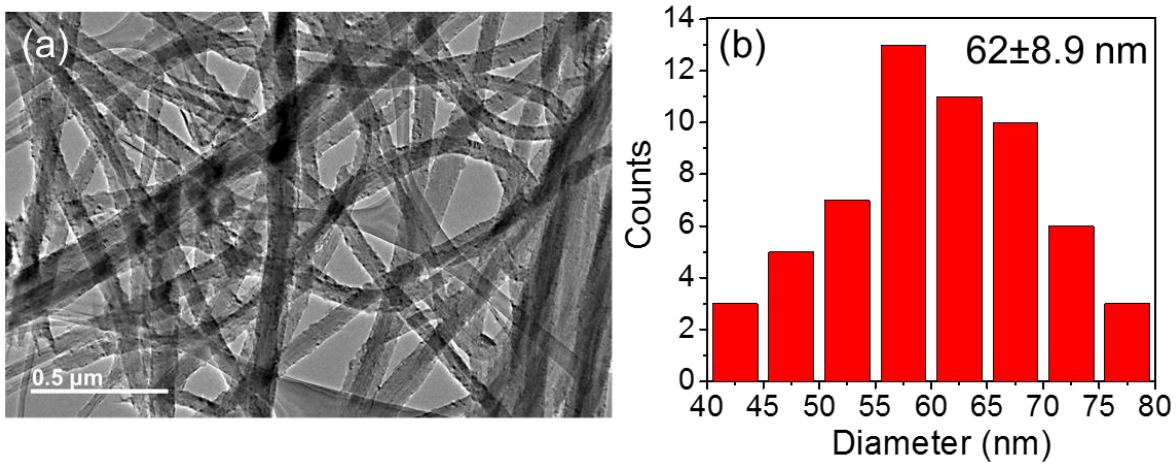

Figure S8. (a) TEM images of W-CNT and (b) statistical analysis of diameter distribution in W-CNT.

Fig. S9 shows the low temperature annealed CNT-PAN by conventional furnace: 1273 K for 2 h with a heating rate of 10 K/min. The furnace heating not only is less efficient in energy and time consumed but also lead to amorphous structure owing to lower temperature is in-sufficient to fully graphitize the PAN into highly crystalline carbon.

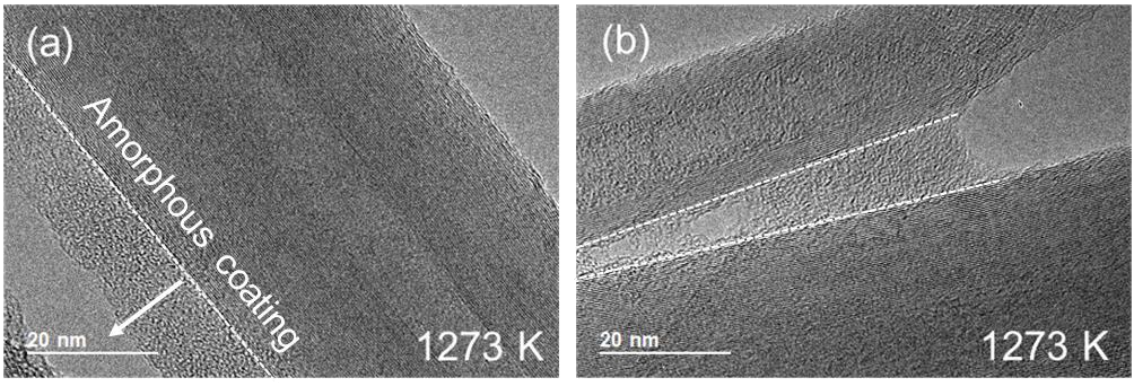

Figure S9. (a)-(b) TEM images of CNT-PAN after annealed at 1273 K for 2 h by conventional furnace heating. The coating layers still show amorphous/disorder structure owing to lower carbonization temperature utilized.

Microstructures of W-CNT (0.5%PAN)

As shown in Fig. S10, the lower concentration PAN (0.5% in DMF) cannot uniformly coat all the fibers, which may be due to the low concentration solution becoming discontinuous after totally drying. Most of CNT fibers in W-CNT (0.5%) are bare or only partially covered with a carbon coating. Thus, the "glue-and-welding" effect is limited.

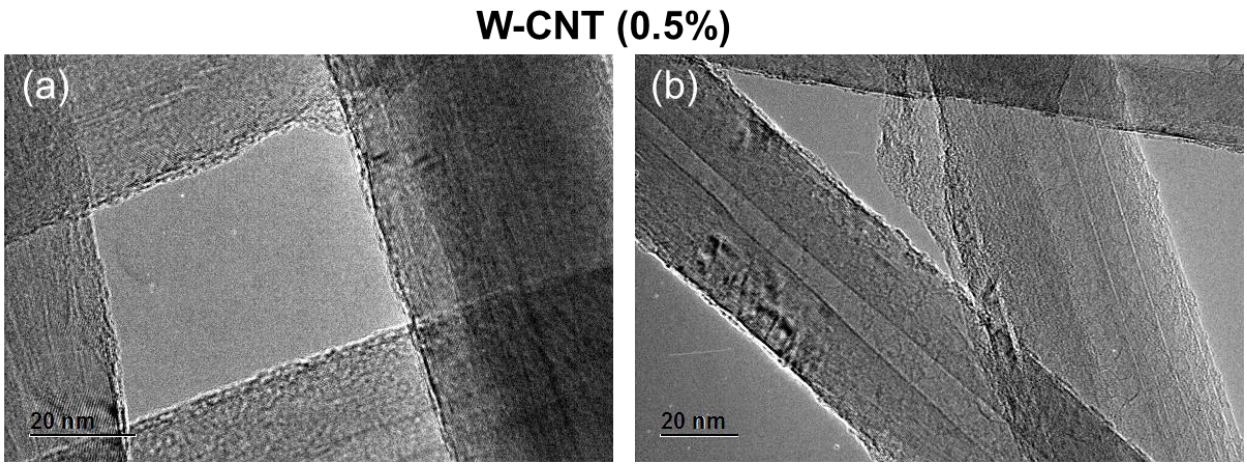

Figure S10. (a) and (b) TEM images of W-CNT welded using a 0.5% PAN solution.

5% PAN coating

As the concentration of PAN increased to 5%, it becomes more viscose and will cause problems for the conformal coating onto CNT film. As shown in Fig. S11, the 5% PAN polymer can form a separate polymer layer on top of CNT film. After the high temperature annealing, clear graphitic layers are formed on top of the CNT film, separating with the backbone CNT film. The conductivity of W-CNT-5 is ~ 700 S/cm which is statistically lower than W-CNT-2. We believe this is due to the increased thickness of the W-CNT film as well as the negative effects of the less compact graphitic layers from PAN coating (Fig. S11d). Besides the conductivity, the graphitic layers are also brittle since there are no CNTs embedded for mechanical enhancement.

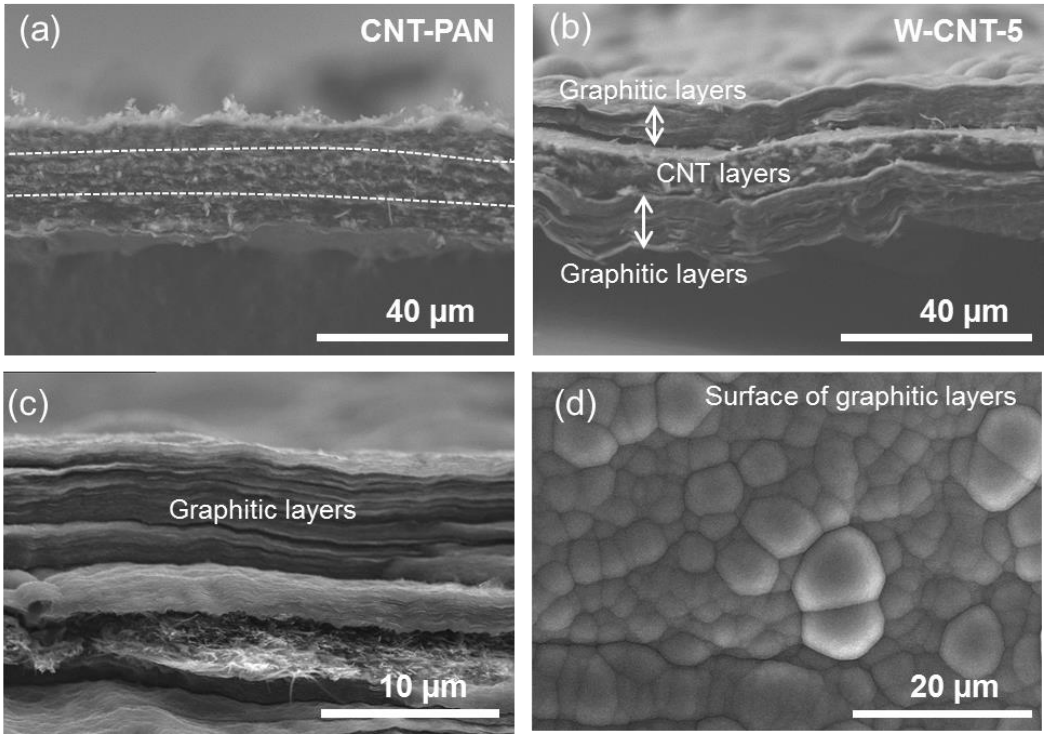

Figure S11. SEM images of (a) CNT-PAN and (b) W-CNT using 5% PAN solution. (c) - (d) Magnified SEM images of the graphitic layer and surface of the graphitic layer. The SEM image of W-CNT-5 shows the formation of graphene layers on top of the CNT film, as the viscose PAN tends to stay on top of CNT film instead of being absorbed onto individual CNTs.

Corrosion measurement of ACC and CNT

The commercially available activated carbon cloth (ACC) current collector was also evaluated using the same conditions of those for the W-CNT film. Fig. S12 shows the ACC carbon is relatively stable in alkaline solutions at both anodic and cathodic conditions, revealed by the similarity of initial CV and CV after 48 h stressing. The differences between initial CV with later ones are due to the initial wetting process of carbon with the aqueous electrolyte. In acid electrolyte, however, ACC carbon is not stable especially at cathodic potential as shown in Fig. S12d with increased map areas inside CV. The strong oxidative corrosion at cathodic potential leads to the oxidative corrosion of ACC.

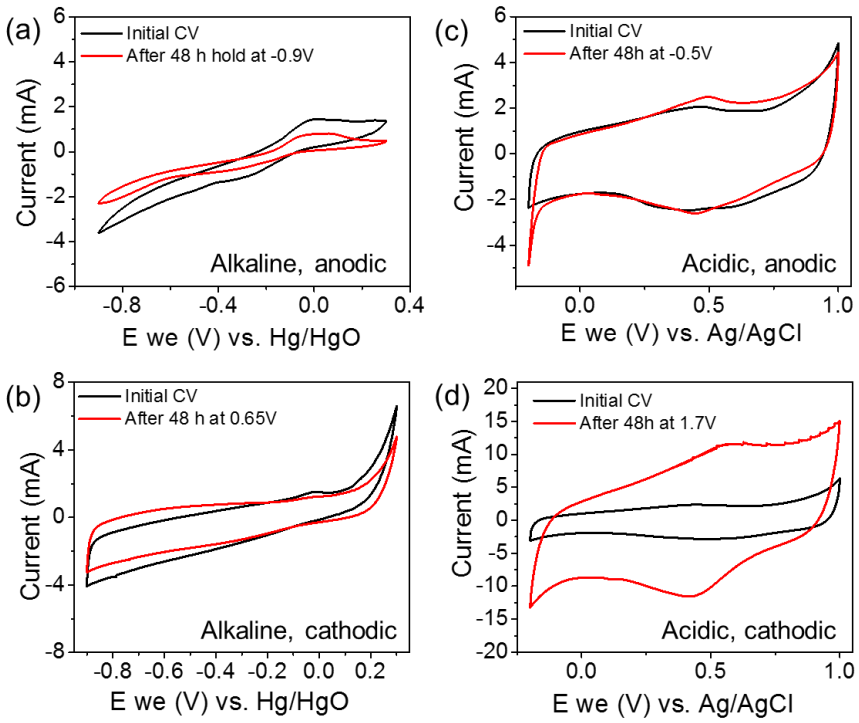

Figure S12. Corrosion evaluation of commercially available ACC carbon. CV before and after holding the W-CNT film in alkaline electrolyte at (a) -0.9 V (anodic potential) and (b) 0.65 V (cathodic potential) (*vs.* Hg/HgO); and in acidic electrolyte at (c) -0.5 V (anodic potential) and (d) 1.7 V (cathodic potential) (*vs.* Ag/AgCl).

We have also measured the potentiostatically stressing of CNT film as a comparison with W-CNT film. From the corrosion result of W-CNT and ACC carbon, the extreme corrosion condition occurred when potentiostatically stressing at a cathodic potential (1.7 V) in strong acid (5 mol/L H_2SO_4). We therefore chose this condition to stretch pristine CNT film.

As shown in Fig. S13a, the CNT film is placed into the T-cell setup. The fixed electrodes geometry in T-cell ensures the accuracy of multiple CV measurements during the potentiostatically stressing. Fig. S13b shows the initial CV and CV after CNT film stressed for 12 hours at 1.7V in 5 mol/L H_2SO_4 (cathodic potential in acidic conditions). There is a slightly increase in the area of CV and the Q/HQ redox peak height, indicating the increased corrosion as compared to the pristine CNT film. However, we are unable to test CV for 24 h and 48 h for comparison, owing to the brittleness of CNT film in highly corrosive conditions; the catalytic evolution of oxygen evolution when stressing at 1.7 V also plays a critical role. The initial CNT film becomes broken and we found CNT dispersed in the electrolyte after 24 hours of stressing (Fig. S13c).

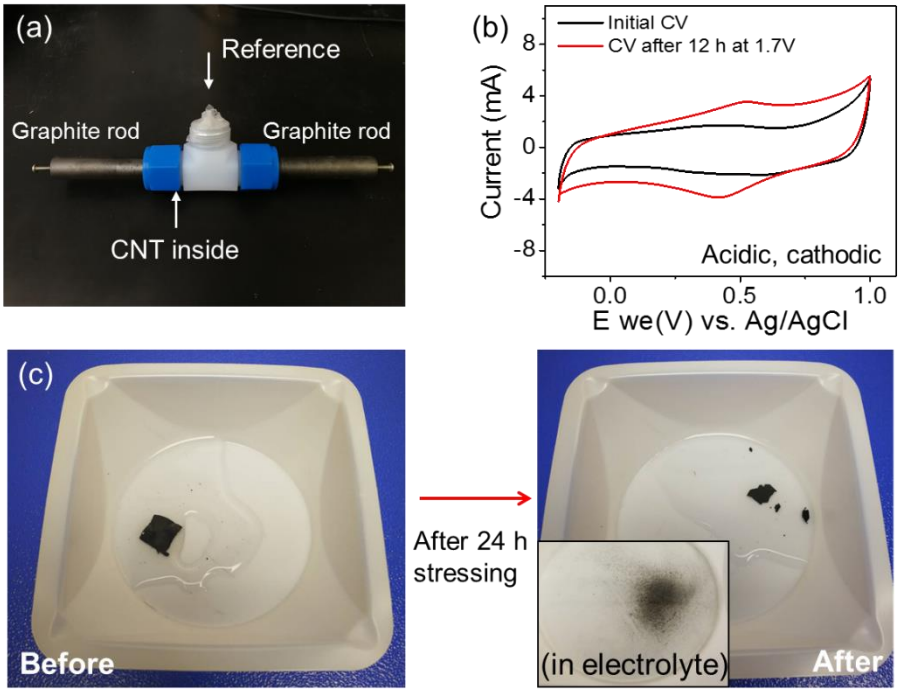

Figure S13. Corrosion measurement of pristine CNT film. (a) T-cell for corrosion measurement. (b) CV test of initial CNT film and after potentiostatically stressing for 12 h at 1.7 V in 5 mol/L H_2SO_4. (b) The photo images of broken CNT film after stressing for 24 h. Some dispersed CNTs were found in the electrolyte.

Therefore, pristine CNT may be stable in these corrosive conditions owing to its high crystallinity, however, the brittleness of CNT film originating from the poor interactions among CNTs leads to very weak mechanical properties that cannot stand for long corrosion stressing.

Properties after corrosion

From the cyclic voltammetry (CV) test (main text Fig. 4), W-CNT film shows stable performance after 48h potentiostatically stressing in strong acidic/alkaline conditions, indicating the stable structure of the W-CNT film in these harsh corrosive environments. We have also conducted both TEM and Raman for the W-CNT films soaked in acid solution after 48h potentiostatically stressing at cathodic potentials, as this condition is found to be the most challenging condition revealed by the CV test. As shown in Fig. S14a, the film is still intact after the potentiostatically stressing. The Raman spectra show an increasing in D peak, however, an indication of slightly increasing in defect concentration (at least surface defects) after stressing (Fig. S14b). We also performed TEM characterizations. The epitaxial layers (EL) and welded junction between CNTs are still clear and maintained after stressing (Fig. S14c). In addition, low magnification TEM images show that the CNTs are still in the interconnected structure. Overall, the W-CNT film is still in good shape and welding junction are still clear.

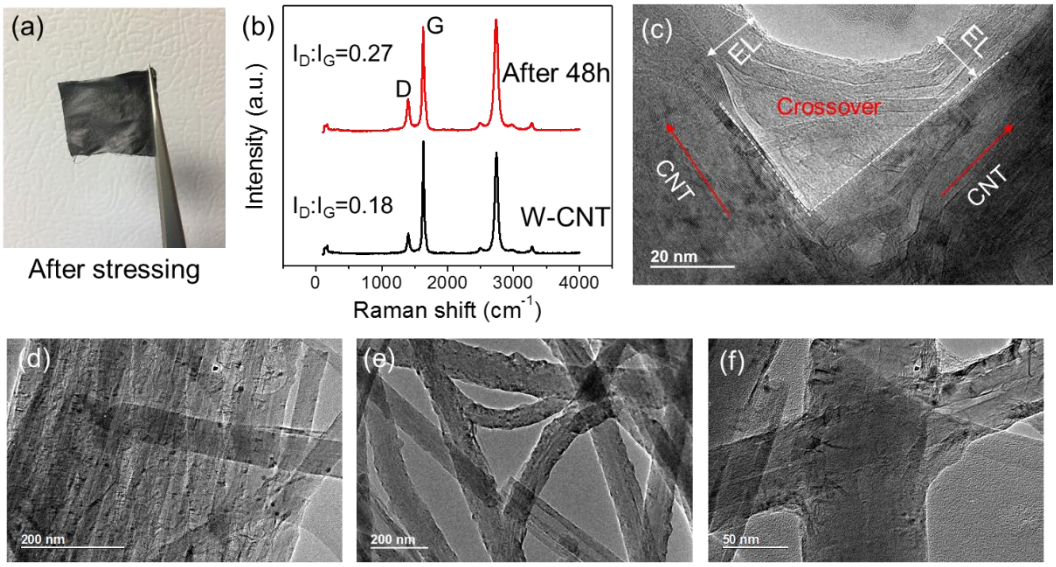

Figure S14. (a) Photo image, (b) Raman, and (c)-(f) TEM images of the W-CNT film after 48h stressing in acid solution at cathodic potentials. The Raman spectrum after stressing has an increasing D peak, indicating the slightly increasing of (surface) defects. In addition, the TEM images show the welding structures are still maintained.

Applied to other CNT substrate

We have also applied the "epitaxial welding" process to a random oriented CNT film prepared using vacuum filtration of CNTs solutions. The CNTs were synthesized by conventional chemical vapor growth. The resultant CNTs were treated by nitric acid to increase the surface polar groups and therefore improved water wettability. The final CNT film was prepared by vacuum filtration of CNTs in aqueous suspension (Fig. S15a). As the film prepared by vacuum filtration is more compact than aligned CNT film used in our main text, we used 0.5% PAN solution for polymer soaking and conformal coating.

The initial picture of vacuum filtrated CNT film is shown in Fig. S15a. We then cut the film into a rectangular shape for PAN coating and followed by high temperature annealing as demonstrated in Fig. S15b. After the annealing, the high crystallinity in the W-CNT film is confirmed by the Raman spectra (Fig. S15c). The pristine CNT has a relatively larger D peak and after the high temperature annealing, the crystallinity is further improved as indicated by the decreasing of D peak (I_D/I_G decreased from 0.28 to 0.1).

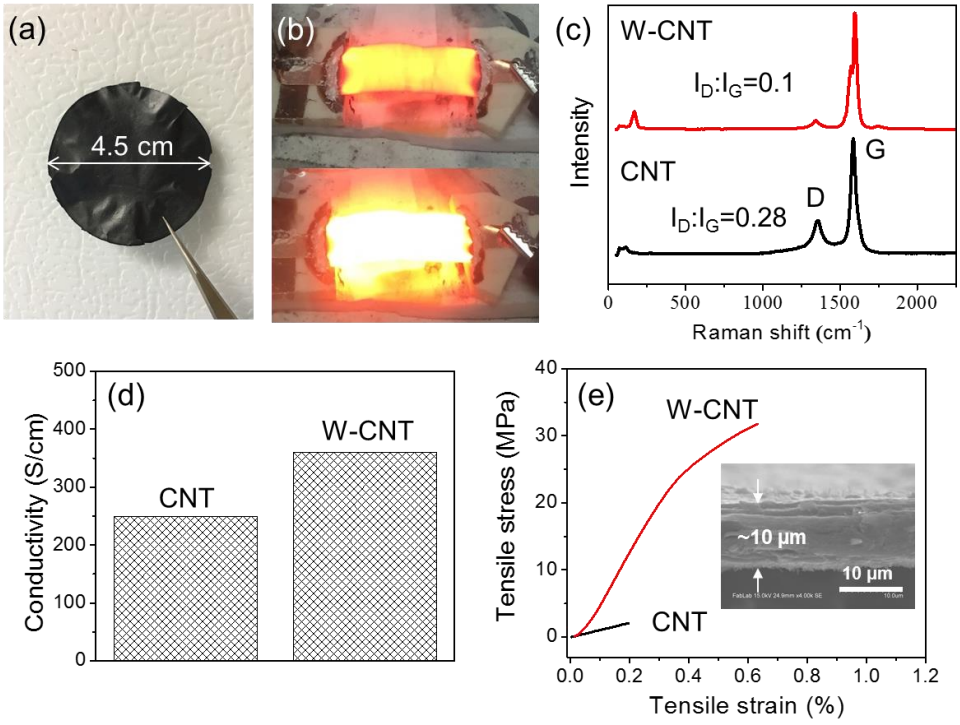

Figure S15. (a) Digital images of P3-CNT film and (b) the PAN coated CNT film during the high temperature annealing. (c) Raman spectra, (d) conductivity and (e) stress-strain measurements for pristine CNT and W-CNT film. The inset shows the thickness of pristine CNT film (~10 μm).

The conductivity increased from ~250 S/cm for CNT film to ~360 S/cm for W-CNT (Fig. S15d). In addition, the mechanical strength increased from ~2 MPa to ~30 MPa after rapid high temperature annealing (film thickness ~10 μm, Fig. S15e). The pristine CNT film is brittle and breaks at the initial stage of strain-stress measurement, while after welding, the mechanical performance of the W-CNT film has been significantly improved.

We also characterized the microstructure evolution in the epitaxial welding process (Fig. S16). The CNT-PAN sample (before annealing) shows intertwined CNTs scaffold with few PAN polymer aggregates. After high temperature annealing, the CNT film becomes neat and shows a well-defined CNTs that are also intertwined/welded together. The fiber diameter increased as an epitaxial growth process. The improved conductivity of W-CNT film also gives better image quality. In the meantime, the CNT welding is also clear at the junction points.

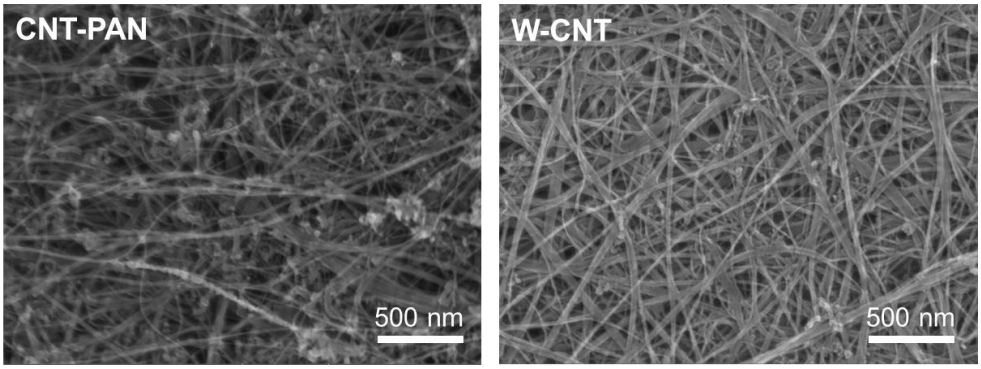

Figure S16. SEM images of CNT-PAN film and W-CNT film (after high temperature annealing).

The above data suggests that the “epitaxial welding” method is very effective in achieving highly crystalline, junction welded CNT films with both improved conductivity and mechanical properties, demonstrating the generality of our method for various carbon nanomaterials.